Magnetic record of El Niño Southern Oscillation in Late Pleistocene sediments from Mucubají Lake (western Venezuela)

JUAN ANDRÉS ARÉVALO GROENING[1], VINCENZO COSTANZO-ALVAREZ[1], MILAGROSA ALDANA[1], EDUARDO CARRILLO[2] AND FRANCK AUDEMARD[3]

1 Universidad Simón Bolívar, Departamento Ciencias de la Tierra, Sartenejas, Caracas 1080, Venezuela (vcosta@usb.ve)

2 EECP Geosciences, Katy, TX 77494, USA

3 Fundación Venezolana de Investigaciones Sismológicas, FUNVISIS, El Llanito, Caracas 1070, Venezuela

Received: April 13, 2016; Revised: October 12, 2016; Accepted: December 19, 2016

ABSTRACT

El Niño Southern Oscillation (ENSO) is an internal forcing of the climate system. This event has an actual frequency of 2 to 8 years. Evidence from a paleoclimate proxy database of gray scale (GS), in samples from Pallcacocha lake in Ecuador, indicates that the ENSO had a frequency of 35 to 75 years during the Late Pleistocene. In this work we explored the possible relationship between the ENSO proxies (GS) from Pallcacocha and magnetic parameters from sediments sampled at the Mucubají lake in Mérida, Venezuela (i.e. mass-specific magnetic susceptibility, magnetic remanence S ratio and susceptibility-normalized saturation isothermal remanent magnetization). After applying a Lanczos bandpass filter to the rock magnetic and the GS data, in order to remove, as much as possible, frequencies associated to any periodic event other than ENSO, we found significant correlations between GS and magnetic parameters for the period between 12450 and 10560 cal. yrs BP. These relationships were obtained using an Adaptive Neuro Fuzzy Inference System (ANFIS), a hybrid algorithm that combines fuzzy logic with neural networks. The results show that the magnetic parameters obtained in Mucubají are able to explain 50.5% of the total variance of the ENSO proxy in a range of 35 to 75 years in Pallcacocha, which is roughly the same percentage of the total variance of the temperature in the Venezuelan Andes, explained by the ENSO at present times. In this way we have inferred a possible influence of the ENSO in the Venezuelan Andes during the Late Pleistocene.

Keywords: paleoclimate, Pleistocene, El Niño, neuro fuzzy, rock magnetic proxies, lake sediments

1. INTRODUCTION

El Niño Southern Oscillation (ENSO) is a mode of variability of the climate system, wherein ocean and atmosphere act synchronously, resulting in decadal and inter annual scale climate changes. The ENSO is well known for producing one of the most consistent relationship between abnormal patterns of rainfall and temperature changes in northern South America (*Ropelewski and Halpert, 1987*). In the Venezuelan Andes, the ENSO signal is clear cut, explaining 20% to 50% of the rainfall and 50% of the temperature total variance in that region (*Cárdenas et al., 2002 and 2003*). In fact, the occurrence of warm (or cold) phases results in either a deficit (or excess) of precipitations and higher (or lower) temperatures.

Paleoclimate evidence from the temperature variation of the sea surface (*Koutavas et al.,2002*; *Kienast et al., 2006*), and the frequency and intensity of the ENSO (*Rodbell et al., 1999*; *Moy et al., 2002*) suggests that the climatic conditions perceived in the past, at the equatorial Pacific, were not similar to those observed at present. Indeed, there is evidence that the ENSO behaved differently during the Late Pleistocene and Holocene. Using global climate models it was found that the change in the amount of solar radiation, incident on the top of the atmosphere due to the precessional cycle (Milanković forcings), is capable of affecting the system generating different climate states that change significantly the frequency and intensity of the ENSO (*Clement et al., 1999,2000,2001*).

By examining the role of the ENSO as a source of abrupt changes in the climate system, it was demonstrated that, under similar orbital configurations, it remained inactive twice in the last 500000 cal. yrs BP, namely during the Younger Dryas (ca 12000 cal. yrs BP), and 400000 years ago (*Clement et al., 1999,2000,2001*; *DeWitt and Schneider, 2000*; *Otto-Bliesner et al., 2006*; *Timmerman et al., 2007*). Reconstructions of sea surface temperatures (SST) in the eastern end of the equatorial Pacific, estimated via series of Mg/Ca and $\delta^{18}O$ in foraminiferae, indicate that they have varied over the past 30000 years, when the seasonality was modulated by the precessional cycle (*Koutavas et al., 2002*). This evidence confirms the "sensitivity" of the climate system to the Milanković forcings. Paleotemperatures of the eastern end of the equatorial Pacific, estimated from $\delta^{18}O$ in unsaturated alkenone, show that between 16500 and 14500 cal. yrs BP, as well as between 12500 and 11500 cal. yrs BP, the sea surface was colder than it is today, supporting the idea that during these periods the ENSO was less active (*Koutavas et al., 2002* and *Kienast et al., 2006*).

This work investigates whether or not the actual effects of the ENSO upon the rainfall regime and temperature changes in the Venezuelan Andes, are similar to those that prevailed in the region during Late Pleistocene times. Therefore, we look for a set of numerical relationships that might predict the likely connections between magnetic paleoclimate proxies in Late Pleistocene sediments from Mucubají lake (Venezuela), with an ENSO paleoclimate proxy obtained by *Rodbell et al. (1999)* in sediments from the Pallcacocha lake (Ecuador) for that time period. The ENSO proxy consists in a gray scale (*GS*) available from the paleoclimatic database of the National Oceanic and Atmospheric Administration NOAA (*Rodbell et al., 1999*). The magnetic parameters obtained in Mucubají lake were: mass-specific magnetic susceptibility χ, magnetic remanence *S* ratio and susceptibility-normalized saturation isothermal remanent magnetization $SIRM/\chi$.

Magnetic susceptibility has been extensively applied as a paleoclimate proxy in the past, since the pioneering works by *Shackleton and Opdyke (1973)* and *Kent (1982)* in marine sediments, up to the numerous studies carried out in lake sediments (e.g., *Hu et al., 2000*; *Li et al., 2006*; *Wang et al., 2010*; *Tamuntuan et al., 2010*; *Zhang et al., 2012*; *Su et al., 2013*; *Duan et al., 2014*; *Hayashida et al., 2015* among others), that also include other magnetic parameters as paleoclimate proxies (i.e. *SIRM* and anhysteretic remanent magnetization *ARM*).

Because the complexity of the problem we are dealing with, an adaptive neuro fuzzy inference system (ANFIS), that combines fuzzy logic with neural networks, was applied to obtain a set of non linear empirical relationships between magnetic and ENSO paleoclimate proxies. The ANFIS has been widely used in geosciences (i.e. *Hurtado et al., 2009*; *Ziaii et al., 2009*; *Rajaee et al., 2010*; *Singh et al., 2010*; *Tahmasebi and Hezrkhani, 2010* and *Zoveidavianpoor et al., 2013*, among others). Specifically in paleoclimate studies, the ANFIS was previously applied to establish non linear relationships between magnetic parameters and $\delta^{18}O$ proxies by *Da Silva et al. (2010)* and *Peralta et al. (2013)*. *Da Silva et al. (2010)* found some non linear relationships between Miocene global climatic changes (benthic foraminifera $\delta^{18}O$) and magnetic parameters from a Colombian stratigraphic well. *Peralta et al. (2013)* investigated the correlation between the magnetic footprint obtained for a section of the Quaternary sedimentary fill in Mucubají lake, and global climate changes in the northern Atlantic between 13000 and 10700 cal. yrs BP/

2. GEOMORPHOLOGICAL AND CLIMATIC SETTING

The Mérida Cordillera is located in the Venezuelan Andes, between 8.5°N and 9.8°N (Fig. 1a). The climate in this region is dominated by the movement of the Intertropical Convergence Zone (ITCZ) which follows the seasonal cycle of solar declination.

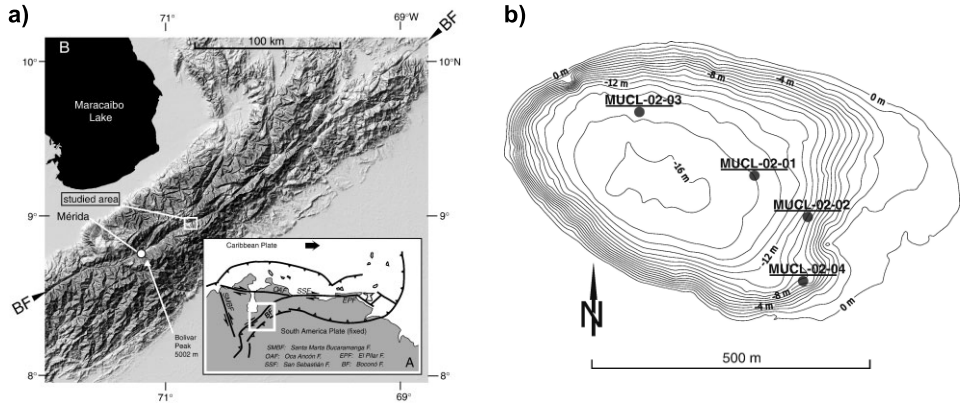

Fig. 1. **a)** Regional geographical and structural setting of the Mucubají lake in western Venezuela, and **b)** bathymetric map of Mucubají lake showing the location of all the sampling sites including MUCL 02-01 for this study (*Carrillo et al., 2008*, © 2007 Elsevier B.V.).

The Mucubají valley shows at its top a glacial cirque, formed during Pleistocene times, with lateral moraines extending down to the valley. The regional strike of the whole area is NNW; however, the moraines have a NE strike in the Mucubají lake, following the direction of the Santo Domingo river valley (*Stansell et al., 2005*). Mucubají lake is located at an elevation of 3550 m a.s.l. and has a perimeter of approximately 2.3 km, 785 m length, 450 m width, 16 m maximum depth and a water volume of 1.5 million m^3 (*Carrillo et al., 2008*). These dimensions could vary depending on the annual rate of precipitation.

Due to its location, the study area contains information of natural events that depend on the climate and its variability, such as glacial processes in the basin of the lake. The presence of moraines formed during the Little Ice Age (*Polissar et al., 2006*) is an indication of the sensitivity of this region to climate changes. The Mucubají creek, a major tributary of the lake, descends directly from the top of the valley. There is no body of water along its pathway, so clastic sediments trapped in the lake are a good indicator of environmental changes occurring upstream.

3. METHODOLOGICAL FRAMEWORK

3.1. Sampling

Two adjacent piston cores (MUCL 02-01-02 and MUCL 02-01-03), collected at no more than few centimeters of lateral separation between them, make up the combined MUCL 02-01 section. These cores were taken from the bottom of the Mucubají lake at about 14 m deep (*Carrillo, 2006* and *Carrillo et al., 2008*). Figure 1b shows the bathymetry of Mucubají and the location of the MUCL 02-01 sampling site, just on the steep southeastern slope of the basin. Ten grams of sample were cut each 2 cm along MUCL 02-01-02 and MUCL 02-01-03 cores, and then prepared in cubic plastic boxes of 10 cm^3 each. Due to their proximity, both cores comprise exactly the same lithological sequence. Thus, a combined stratigraphic section was assembled taking into consideration the overlap between MUCL 02-01-02 and MUCL 02-01-03 (Fig. 2a), that comprises a total of 92 cm (46 samples). The combined MUCL 02-01 section lies within a depth interval that goes between 101 to 555 cm (227 samples), down from the top of the entire stratigraphic column (Fig. 2b). In addition, a turbiditic interval that goes from 109 to 123 cm (8 samples), was completely removed from this section (Fig. 2b). Such a removal was justified since the mineralogical characteristics and average particle grain-size of this interval correspond to a shock-induced deposit or a reworking feature, likely related to an allegedly instantaneous seismic episode at the nearby Boconó Fault (*Carrillo, 2006* and *Carrillo et al., 2008*).

Figure 2b shows a lithostratigraphic summary of the entire MUCL 02-01 column. The main units described by *Carrillo et al. (2008)* are:

- Unit I: sandy and shale siltstones, with lamination or thin inter-stratification and layers of basal horizons, with fine to medium-grained sands (quartz, muscovite and feldspars). The bottom of this unit shows a layer of coarse-grained and massive shale that underlines another one of coarse-grained sands.

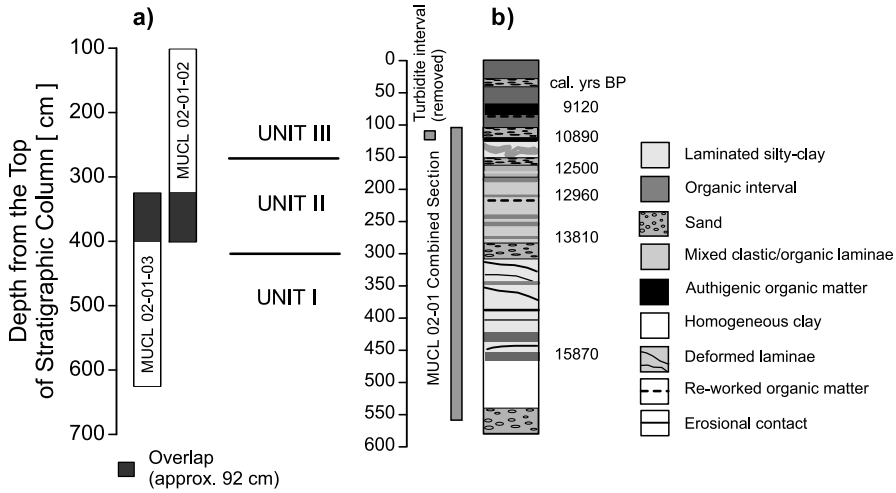

Fig. 2. **a)** Outline of the stratigraphic intervals comprised by cores MUCL 02-01-02 and MUCL 02-01-03 from Mucubají lake. Both of them make up the combined MUCL 02-01 section used in this study. **b)** Complete stratigraphic column for MUCL 02-01, showing the main lithological features at this sampling site, along with the ^{14}C intersection ages, obtained from the 2σ (95%) interval and the highest mode of intersection between the ^{14}C conventional age and the calibration curve; the span of the combined MUCL 02-01 section and the shock-induced turbidite interval (after *Carrillo et al., 2008*, © 2007 Elsevier B.V).

- Unit II: sandy to silty shales with particles of organic matter. Radiocarbon ages for this unit, in this core, show that the transition from Unit I to Unit II approximately coincides with the end of the Last Glacial Maximum (LGM).
- Unit III: mainly silt, shale and abundant organic matter, without a clear stratification.

3.2. Rock magnetic measurements in Mucubají lake

We used a Bartington MS2 system to measure the room-temperature magnetic susceptibility for the samples taken along the combined MUCL 02-01 section. The readings were repeated 5 times and a standard deviation of less than 10% was obtained for each sample. We also calculated χ, $SIRM/\chi$ and S ratio $S = IRM_{-0.3\,T}/SIRM$ (*Bloemendal et al., 1992*). $IRM_{-0.3\,T}$ is *IRM* measured after application of field of 0.3 T in direction opposite to *SIRM*, *SIRM* being measured after application of field of 3 T. These measurements were performed using a Molspin minispin rock magnetometer with sensitivity better than 1×10^{-4} A/m at 24-s time constant. The *SIRM* was acquired using an ASC IM-10-30 pulse magnetizer with interchangeable coils, capable of generating fields up to 3 T. Figure 3 shows these experimental values for each 2-cm sampling interval.

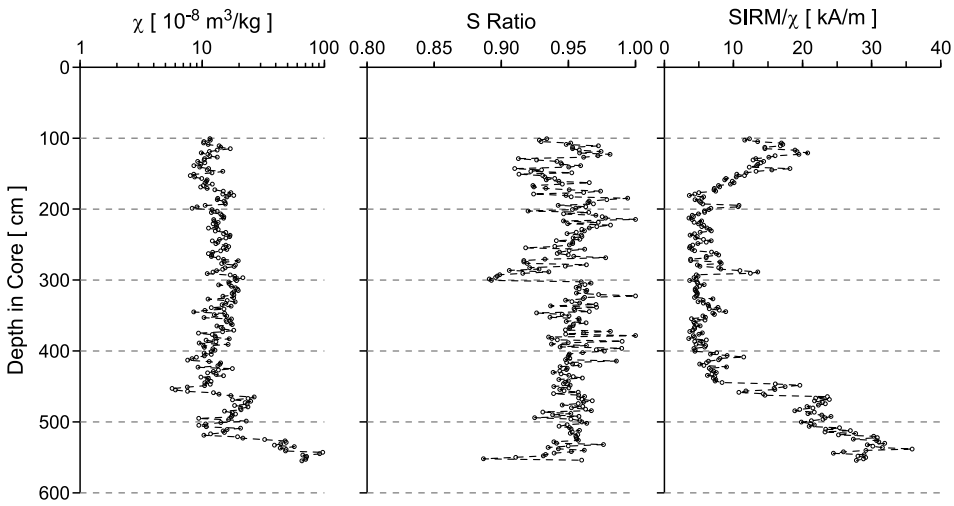

Fig. 3. Experimental values for each 2-cm long sampling intervals along the combined Mucubají section MUCL 02-01. χ - mass-specific magnetic susceptibility; magnetic remanence S ratio $S = IRM_{-0.3\,\mathrm{T}} / SIRM$; $IRM_{-0.3\,\mathrm{T}}$ is IRM measured after application of field of 0.3 T in direction opposite to $SIRM$, $SIRM$ is saturation isothermal remanent magnetization.

3.3. Age-depth calibration of Mucubají and Pallcacocha data

The age-depth relationship along the complete MUCL 02-01 column was estimated by *Carrillo (2006)* based on accelerator mass spectrometer (AMS) ^{14}C analyses (Fig. 2b). These ages were obtained for the fraction of organic matter extracted from the whole rock, at different stratigraphic levels, and then calibrated using the OxCal v3.9 program (*Bronk Ramsey, 2001*). The organic matter had two possible origins, namely in situ aquatic production and/or reworking of the watershed by peat bogs and organic soils. Terrestrial plant detritus were not identifiable in these samples. Additionally, when working on sediments of a lake with the characteristics of Mucubají, a correction related to a possible reservoir effect has to be applied. This correction depends on the isotopic data of the carbon content in the water and on an estimation of its residence time (*Stuiver et al., 1998*). Figure 2 shows the intersection ^{14}C ages that were obtained using the 2σ (95%) interval and the highest mode of intersection between the ^{14}C conventional age and the ^{14}C calibration curve (*Carrillo, 2006* and *Carrillo et al., 2008*). These ages were employed as chronological tie-points (cal. yrs BC) along the entire MUCL 02-01 stratigraphic column. According to these data, *Carrillo (2006)* concludes that there are two rates of accumulation, namely one of 0.77 mm/yr corresponding to the period 15870–12500 cal. yrs BP (i.e. 470 and 175 cm), and another one of 0.23 mm/yr for the period 12500–10890 cal. yrs BP (i.e. 176 and 120 cm). Thus, the minimum time-resolution of each 2-cm sample, for the first time interval, is 32 years, and 108 years for the second one.

In order to analyze the influence of the ENSO on the Mucubají lake sediments, we need a complete record of some paleoclimate proxy obtained from a location directly linked to this event. Thus we have tied up Mucubají magnetic parameters to a time series of gray scale (*GS*), recorded in a 9.2-m core from the Pallcacocha lake in southwestern Ecuador (*Rodbell et al., 1999*). Pallcacocha lake has been clearly influenced by the ENSO due to its proximity to the Pacific Ocean and, like Mucubají, is located in a mountainous tropical region. Moreover, this lake formed by glaciers melting, in a similar geological setting to the one that prevailed in Mucubají at the end of the Pleistocene and beginning of the Holocene.

To obtain the *GS*, a sediment core is digitally photographed. The images are processed with a graphic program that attaches to each pixel a numerical value between 0 (completely white) and 256 (completely black), in direct relation to the weight percentage of carbon. The total carbon content between a pair of ^{14}C-dated sedimentary layers, is used to determine an average accumulation rate. This rate makes it possible to assign a deposition time to each stratum, within the full range of shades of gray enclosed by the two ^{14}C tie-points. That is to say, the lighter the color of the layer, the lower the accumulation time. The width/time resolution of the age-calibrated *GS* could be as high as 0.1 mm (sub annual). In Pallcacocha, each pixel represents 0.3 mm of the core. Since the *GS* is a good proxy for carbon content, that records the oscillation between inorganic, storm-induced-clastic and organic-rich sedimentation, it also stands as an optimal high-resolution paleoclimate proxy. Indeed, according to *Rodbell et al. (1999)* the sedimentation of inorganic clastic layers was probably related to episodic storms that produced abundant debris flows drained into the lake. From the time-series analysis of the *GS*, and between the Late Pleistocene and the Early Holocene, the periodicity at which these layers appear, lies within two bands of 15–17 and 35–75 years. The 35–75 years band explains more of the *GS* total variance during the Late Pleistocene and is the only ENSO-like signal from 15120 up to 13250 cal. yrs BP (*Rodbell et al., 1999*). After approximately 5000 cal. yrs BP, the recurrence of clastic sedimentation increases up to 2–8 years, which is consistent with the actual ENSO period. In the Pallcacocha strata, accumulated throughout the last 200 years, there is a close age-match between the periodic occurrence of these clastic layers and the historical record of ENSO´s moderate to severe events, previously reported by *Quinn and Neal (1992)*.

The Pallcacocha core covers the last 15000 years with two time gaps around 13300 ± 16 cal. yrs BP and between about 12650 and 12500 cal. yrs BP. Such discontinuities divide the data into the two age intervals shown in Fig. 4, namely 12500 to 10560 cal. yrs BP (Interval 1) and 14770 to 13320 cal. yrs BP (Interval 2). The sedimentation rate estimated for the Pallcacocha lake, for the time period between 15000 and 10000 years, is 0.52 mm/yr. We reduced the stratigraphic/temporal resolution of the original *GS* by taking averages every 40 years (approximately 2.8 cm).

An adjustment was made so that the series of *GS* and the magnetic parameters could have the same time reference within the uncertainties of radiocarbon chronologies. We rounded up available ^{14}C intersection ages for both Mucubají and Pallcacocha, to their nearest tenths and then interpolated the magnetic parameters and the *GS* values using a 10 years time interval by assuming a continuous linear connection between two consecutive magnetic or *GS* actual values. This approach results in a total of 344 input

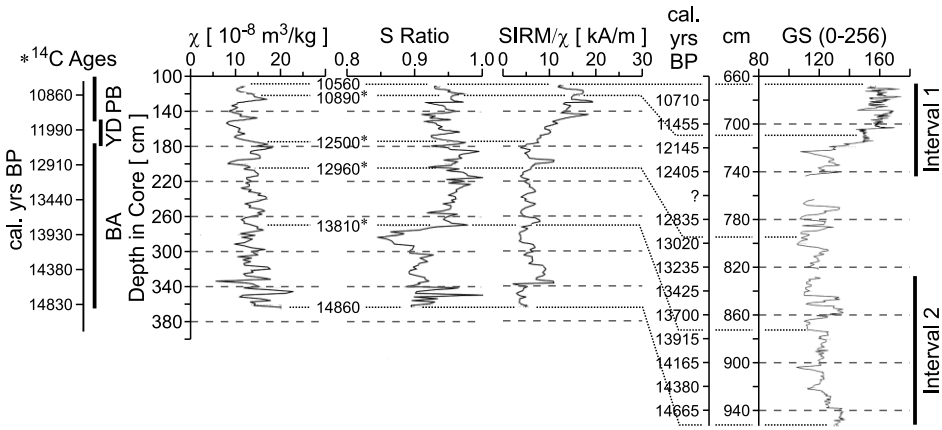

Fig. 4. Age-depth callibration of Mucubají (combined MUCL 02-01 section) and Pallcacocha unfiltered data. Profiles of mass-specific magnetic susceptibility χ, magnetic remanence S ratio $S = IRM_{-0.3\,\mathrm{T}} / SIRM$ and susceptibility-normalized saturation remanence (*SIRM*) (Mucubají) versus stratigraphic level. Profile of ENSO proxy (Pallcacocha) versus stratigraphic level, namely shades of a gray (*GS*), is available from the paleoclimatic database of NOAA (after *Rodbell et al., 1999*). Additional information in this figure includes: intersection ^{14}C age tie points (cal. yrs BC), obtained for the combined MUCL 02-01 section (after *Carrillo et al., 2008*), the time span for the Bolling/Allerød (BA); Younger Dryas (YD) and Preboreal (PB) periods and the two intervals with continuous data, between 12500 and 10560 cal. yrs BP (Interval 1), and from 14770 to 13320 cal. yrs BP (Interval 2).

vectors of rock magnetic and *GS* (190 in Interval 1 and 154 in Interval 2). Figure 4 shows the columns of these magnetic and *GS* values plotted against depth and age. Notice that, in this way, the proxies from both locations were fixed to the same time reference. Moreover, the time series structures were not altered with respect to Fig. 3. In fact, the Fourier transforms of these data sets were obtained in order to determine possible aliasing. No difference between these spectra was found precluding thus a modification of the data due to re-sampling.

3.4. Filtering

According to *Rodbell et al. (1999)* the most conspicuous ENSO signal in Pallcacocha, during the Late Pleistocene and the onset of the Holocene, had a periodicity of 35 to 75 years. Therefore, by knowing the bandwidth where the ENSO signal might be better recorded, we removed, as much as possible, any other events with distinct periods, from the magnetic and *GS* records of both Mucubají and Pallcacocha lakes. This was done by applying a Bandpass Lanczos filter to the series of each magnetic parameter and *GS* (*Duchon and Hale, 2012*). We choose this filter because it performs, in a rather simple way, all the calculations needed to determine the weight function. The main feature of the Lanczos filter is based on the use of sigma factors which significantly reduce the oscillatory Gibbs phenomenon that occurs in the vicinity of a discontinuity, when the

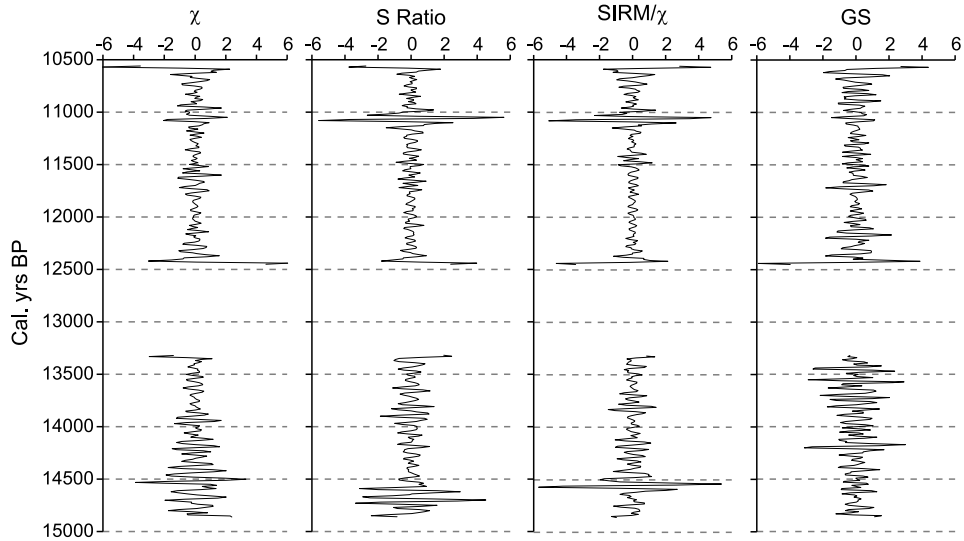

Fig. 5. Profiles of standardized series (i.e. residual values with respect to the corresponding averages) of mass-specific magnetic susceptibility χ, magnetic remanence S ratio $S = IRM_{-0.3\,\mathrm{T}} / SIRM$, susceptibility-normalized saturation remanence (*SIRM*), and grey scale (*GS*) plotted versus ages, after applying a Band Pass Lanczos filter for Interval 1 data (upper row) and Interval 2 data (lower row).

Fourier analysis is carried out. This phenomenon may cause considerable errors in an ideal response function. Figure 5 shows the filtered magnetic and *GS* data from Mucubají and Pallcacocha, for Intervals 1 and 2 respectively.

3.5. Computational methods

Once we tied the paleoclimate section in Mucubají with its Pallcacocha counterparts (i.e. magnetic parameters and *GS*), and both datasets were properly filtered to isolate the possible ENSO footprint, we applied an Adaptive Neuro Fuzzy Inference System (ANFIS) to establish some numerical relationships between magnetic (Mucubají) and paleoclimate (Pallcacocha) proxies. The Fuzzy Inference System (FIS) is obtained from the training of a set of input (magnetic parameters) and output (paleoclimate proxies) variables. We used the modulus ANFIS provided by MatLab. This FIS is equivalent to a Takagi-Sugeno-Kang (TSK) system under some constraints, i.e. a constant or a linear combination of input variables, in addition to a constant term, and an output signal obtained from the weighted average of each output rule (*Finol and Jing, 2002*). A TSK consists of a set of fuzzy if/then rules of the form:

$$R_i\text{: If } x_1 \text{ is } C_{i1} \text{ and } x_2 \text{ is } C_{i2} \text{ and } \ldots \text{ and } x_\mathrm{n} \text{ is } C_{in}$$
$$\text{Then } y_i = c_{i1}x_1 + c_{i2}x_2 + \ldots + c_{in}x_n + c_{i0}$$

In the relationships above, R_i ($i = 1, 2, \ldots, m$) is the i-th fuzzy rule; $C_{i1}, \ldots, C_{in}$ are the antecedent linguistic variables, that define fuzzy sets in the range of the discourse of the

universe, and c_{i1}, …, c_{in} are the consequent parameters. The antecedent fuzzy sets are represented by curves (membership functions), which describe how each point in the input space is mapped to a membership value that ranges between 0 and 1. The parameters that characterize these functions are the premise parameters. To adjust the premise and consequent parameters, ANFIS uses the learning capabilities of neural networks combined with gradient descendent and least square methods (*Demico, 2004*).

The number and type of the membership functions that correspond to each input variable was provided here. The logical operator used to aggregate the input membership sets was the AND operator. Thus, the membership function of every single input variable (in this case we selected a Gaussian curve) is combined, one to one, with the membership functions of the other input variables, resulting in a total number of fuzzy rules that is calculated as the product of the number of membership functions of all the input variables (Grid Partition method).

The level of tolerance between inferred and actual values is fixed beforehand. The epochs are the iterations performed by the program in order to reduce this error; they range from 10000 to 1000. Thus, the training performed by the ANFIS adjusts the parameters of the fuzzy rules and the membership functions as many times as necessary until it either reaches the maximum number of iterations, or the training error keeps under the level of tolerance.

4. RESULTS AND DISCUSSION

4.1. Correlation between Mucubají magnetic and Pallcacocha *GS* paleoclimate proxies: unfiltered data

As mentioned earlier, the *GS* paleoclimate proxy in Pallcacocha is linked to fine-scale lithological variability mostly induced by climate forcings. Likewise, it seems reasonable to argue that the load of magnetic minerals in Mucubají, as well as the distribution of their grain-size, would be also controlled in some extent by the climate conditions in the Venezuelan Andes. Thereby, first and foremost, it is important to have knowledge of the type of magnetic minerals that prevail in the Mucubají samples. In a previous work, *Peralta et al. (2013)* performed thermomagnetic experiments (heating/cooling in air atmosphere), on a set of sediments collected at different stratigraphic levels, from a piston core (i.e. MUCL 02-02) taken 100 meters away from MUCL 02-01 (Fig. 1b). This site is also located in the southern slope of the lake, at depth of about 12 m. MUCL 02-02 samples show a well defined Curie temperature at 580°C, due to the presence of magnetite, plus a minor amount of hematite. There is no evidence for Fe-sulfides in these rocks, namely the characteristic 280–360°C thermal decomposition of greigite into sulfur, marcasite and pyrite (*Sagnotti, 2007*) or the phase transition of hexagonal pyrrhotite above 200°C. Moreover, $SIRM/\chi$ for MUCL 02-01 (present study) are not higher than 35 kA/m. This top value is far below the corresponding averages of 209 and 70.7 kA/m for pyrrhotite and greigite respectively (*Peters and Dekkers, 2003*) precluding thus the presence of these minerals. Additional evidence for the lack of Fe sulfides in the Mucubají sediments comes from the diagenetic precipitation of petal-like crystals of vivianite in the microfactures of the sandy and clayey facies (*Carrillo, 2006*). The presence of this

mineral, a hydrated iron phosphate ($Fe^{2+}Fe_2^{2+}(PO_4)28H_2O$), suggests that these samples are richer in phosphorus than in sulfur. Indeed, vivianite is one of the most stable Fe-phosphates in reducing environments with favorable conditions for bacterial activity, coupled with a high content of iron and a greater ability of the mineral phases for retaining the phosphorus due to the low concentration of sulfates (*Nriagu, 1972*; *Nriagu and Dell, 1974*; *Caraco et al., 1989*).

In such a way, it is reasonable to assume that the χ values, from the Mucubají samples, are a first-order measure of the magnetite content in these rocks. On the other hand, the ratio of concentration-dependent parameters, such as $SIRM/\chi$ and/or $S = IRM_{-0.3\,T}/SIRM$, might result in two first order concentration-independent parameters. So that, these ratios would keep account of the different types of magnetic minerals and/or their corresponding grain-size (*Peters and Dekkers, 2003*) along the combined MUCL 02-01 section. In fact, providing that magnetite is the dominant magnetic phase, the $SIRM/\chi$ will vary inversely to grain-size for samples with similar concentrations of this mineral. Conversely, the *S* ratio, obtained by using a backfield of 0.3 T, should be particularly sensitive to variations in magnetic mineralogies. Nonetheless, it is important to be cautious about such a straightforward interpretation. *Frank and Nowaczyk (2008)* and *Liu et al. (2007)* have demonstrated that the *S* ratio is not always a direct measure of the relative contributions of low and high coercivity magnetic minerals. *Frank and Nowaczyk (2008)* showed that the amount of hematite over magnetite can be quite large in samples with *S* ratio as high as 0.8. Even more, *Liu et al. (2007)* argued that this ratio does not reflect the relative changes in the concentration of antiferromagnetic minerals only. This is particularly true in those rocks with a wide variability of coercivities for both hematite and goethite, coming from different sources.

The χ, *S* ratio, $SIRM/\chi$ and *GS* data used in this work (Fig. 4), cover approximately the period between 14860 and 10560 cal. yrs BP (Late Pleistocene). During that time interval, some major events were associated with global changes in the climate system (*Rull et al., 2010* and *Stansell et al., 2010*). The warm and humid Bolling/Allerød event (BA) occurred roughly between 14600 and 12600 cal. yrs BP and was followed by the Younger Dryas (YD) between 12600 and 11500 cal. yrs BP. Finally, the YD led to the Preboreal (PB) period which lasted until the beginning of the Holocene (approximately 8500 cal. yrs BP).

Magnetic susceptibility χ has been previously considered as a paleoclimate proxy in Mucubají (*Carrillo et al., 2008* and *Peralta et al., 2013*). Indeed, high χ values seem to be related to warm and humid periods (e.g. BA), characterized by the sedimentation of magnetic minerals-loaded terrigenous material, that were brought into the lake by surface runoff and by the Mucubají creek. Conversely, in cold weather (i.e. YD), the intensity of the alteration probably decreased together with χ due to the fact that the climate became dryer and cold.

During the BA the state of the climate in Venezuela was not significantly different from that observed today (*Rull et al., 2010*) favoring the formation of soils. However, during the YD the temperature in the Venezuelan Andes declined sharply (between 2.5° and 3.8°C) and climate conditions became dryer (*Rull et al., 2010* and *Stansell et al.,*

2010). In MUCL 02-01, changes of χ seem to occur at the beginning of the YD with relatively lower values compared with those corresponding to the BA (Fig. 4). *Carrillo (2006)* and *Peralta et al. (2013)* report variations in sedimentation rates and magnetic grain-size in Mucubají, that might be linked to the onset of the YD too.

Differences in the *S* ratio values, between the BA, YD and the PB, also appear to reflect variations in the dynamics of Mucubají lake related to global climate change, as well as to local and regional tectonic events (*Carrillo, 2006*). In the BA, the absolute minimum of the *S* ratio occurs at approximately 14000 cal. yrs BP, signaling a period of major variations in the sedimentation that was possibly triggered by an abrupt draining of the lake, with prevailing oxidizing conditions (*Carrillo, 2006*). After this event, a load of silty-sands accumulated on top of a previously deposited sequence of coarser sediments (*Carrillo et al., 2008*). This granulometric change was registered by an increase of the $SIRM/\chi$ ratios during and after 14000 cal. yrs BP. Approximately 200 years later, *S* ratio values rose and remained more or less constant afterwards, reflecting perhaps a shift towards more reducing conditions and the dominant presence of low coercivity magnetic minerals. After the BA period, the YD cooling is marked not only by a decrease in χ, but also by a decline of the *S* ratio values. A progressive increase of the $SIRM/\chi$, that suggests a drop in the magnetite grain-size, also characterizes this period. After the YD, the $SIRM/\chi$ remained more or less constant during the PB. A similar behavior for these parameters was previously reported for the nearby MUCL 02-02 core by *Peralta et al. (2013)*.

On the other hand, magnetic parameters in Mucubají appear to correlate quite well with some of the general trends observed in the *GS* from Pallcacocha. This paleoclimate proxy have a low mean value all through the BA suggesting more humid and less variable climate conditions for this period. Then, after the YD, a progressive increase of the *GS* values is observed, remaining more or less constant during the PB. Such a behavior is echoed by an increase of the $SIRM/\chi$ ratio that could be related to a progressive decrease of the magnetite grain-size. *Robdell et al. (1999)* argue that the low *GS* values, observed in laminated sediments, correspond to sporadic storms which increased the contribution of terrigenous material into Pallcacocha lake.

In order to quantify the validity and the level of a possible correspondence between the *GS* in Pallcacocha, and the magnetic parameters measured in Mucubají, we firstly determined their connection using linear regression analyses. Table 1 shows the statistical indexes that convey the significance levels of these correlations; they provide some preliminary information of possible climate relationships between the two studied locations (i.e. Pallcacocha and Mucubají). We found meaningful values of the Pearson product-moment correlation coefficient *r* between *GS* and χ or $SIRM/\chi$. However, an acceptable *r* value was not obtained between *GS* and *S* ratio, which could be influenced by different processes unrelated to the variability of the *GS*. Indeed, as mentioned before, in some cases there is a rather complex relationship between this parameter and the relative concentrations of different coercivity magnetic minerals. Moreover, it is important to bear in mind that each proxy represents the footprint of diverse natural processes, such as those related to tectonism in the Venezuelan Andes, which could have affected the Mucubají

Table 1. Correlations between gray scale (*GS*) and magnetic parameters for the whole data collection, together with their corresponding significance levels α. Correlations with $\alpha < 0.05$ are in bold. *r* - Pearson correlation coefficient; χ - mass-specific magnetic susceptibility; *SIRM* - saturation isothermal remanent magnetization; $S = IRM_{-0.3\,\mathrm{T}} / SIRM$.

		χ	S	$SIRM/\chi$
GS	*r*	–0.380	0.072	0.793
	α	**0.000**	0.147	**0.000**

region (*Carrillo, 2006*). Late diagenesis of primary magnetic minerals might have also masked such correlations (*Da Silva et al., 2010*).

Finally, to fully understand the quantitative results of Table 1, it is also necessary to review the global climate context throughout Late Pleistocene times, and its direct effect on the regions under study. During the BA, the Inter Tropical Convergence Zone (ITCZ) in the Atlantic Ocean was probably located over northern South America. Thus, the climate in the Venezuelan Andes might have been humid (*Haug et al., 2001*) and also warm (*Rull et al., 2010*) with a consequent greater input of magnetic minerals and larger χ values. On the other hand, in Pallcacocha, the absence or less frequent ENSO warm phases (*Rodbell et al., 1999*; *Clement et al., 1999,2000,2001*) produced more stable conditions with less precipitation within the BA. In this case, the low numerical values of *GS* could have been due to a higher input of terrigenous material due to changes in the glacial volume that must have prevailed up to about 14000 years (*Rodbell et al., 1999*). Weaker northeast trade winds and the drop of temperature in the sea surface off the coasts of Ecuador (ca. 14000 years ago) kept the eastern Pacific ITCZ in the northern hemisphere. Conversely, the SST in the western Pacific remained almost constant as evidenced by proxies from the South China and Sulu Seas (*Kienast et al.,2006*).

In the course of the YD and the PB, colder and dryer global conditions returned to the Andes and other parts of Venezuela (*Carrillo et al., 2008*; *Rull et al., 2010*; *Bradbury et al., 1981*; *Curtis et al.,1999*) due to the southward displacement of the Atlantic Ocean ITCZ (*Haug et al., 2001*), having an impact upon the wet season. *Zhang and Delworth (2005)* and *Kienast et al. (2006)* argue that the observed cooling of the eastern Pacific during the YD, between South and Central America, was associated to the shutdown of the Atlantic thermohaline circulation. The consequent stronger southern temperature gradient gave rise to the upwelling of colder waters via Ekman transport and the intensification of the trade winds in the eastern Pacific, similar to the ENSO cold phases (La Niña). Although the global climate conditions in northwestern South America were dryer, *Stansell et al. (2005)* argue that a new ice accumulation was observed in Mucubají during the YD, with ice retreat during the PB about 11000 years ago. Today, there are only two seasonal periods in the Venezuelan Andes, namely the rainy and the dry one. The effects on rainfall by the ENSO's cold phase (i.e. La Niña) are more pronounced during the dry season, with a consequent increase of rainfall and the drop of average temperatures in the region (*Cárdenas et al., 2003*). In the same way, it is reasonable to believe that throughout the YD, a rather La Niña-like event may have been the key driver for those ice accumulations in Mucubají.

Due to colder SST in the coasts of Ecuador, throughout the YD and PB periods, the eastern Pacific ITCZ should have stayed in the southern hemisphere (*Zhang and Delworth, 2005*) which is consistent with an increase of the *GS* values observed in the Pallcacocha lake sediments, whereas the absence of glaciers limited the supply of terrigenous material into the lake. The paleoclimate proxies used by *Koutavas et al. (2002)*, *Stott et al. (2002)* and *Kienast et al. (2006)* (i.e. Mg/Ca, $\delta^{18}O$ of G. sacculifer alkenone unsaturation index $U_{37}^{K'}$) show that during the YD and the PB, the zonal gradient of the SST decreased due to a cooling in the western Pacific warm pool. Thus, the cold and dry climate conditions were preserved in the western mountains of Ecuador and the configuration observed during this period, seems to be due to a precessional forcing coupled with the seasonal cycle (*Clement et al., 1999,2000,2001*; *Cane, 2005*; *Otto-Bliesner et al., 2006* and *Timmerman et al., 2007*).

4.2. Correlation between Mucubají magnetic and Pallcacocha *GS* paleoclimate proxies: filtered data

So far, we have focused our attention on the correlations and general trends observed, for the Pallcacocha and Mucubají unfiltered data, throughout the three major periods of climate change that mark the end of the Pleistocene and the beginning of the Holocene (i.e. BA, YD and PB). However, it is important to bear in mind that, when dealing with the ENSO frequency, we are looking at a fine scale climate variability that could induce anomalies in the patterns of rainfall and temperature, independently of the global climate context. *Rodbell et al. (1999)* argue that the ENSO frequency has increased progressively mostly in the last 7000 years (e.g. at present 2–8 years). However, changes in that periodicity have occurred since over 15000 years ago. Prior to 7000 years, the ENSO had a lower frequency of about 15 years. Indeed, between 15120 and 7000 years (Late Pleistocene - Early Holocene) the ENSO was apparently less frequent than today (i.e. < 15 years, up to 75 years).

Correlations between the filtered series of *GS* and χ, *S* ratio and $SIRM/\chi$, using linear regression analyses, indicate statistically significant (α level less than 0.01) relationships for these parameters in Interval 1 (Table 2, Fig. 4). Conversely, these correlations are not significant in Interval 2. Thus, at least for Interval 1, the χ, *S* ratio and $SIRM/\chi$ magnetic proxies might have recorded some of the ENSO signal and could be regarded as good predictors of the numerical values assigned to the *GS*. The anticorrelation observed in Interval 1, between *GS* and χ, seems to be contradictory at first sight; however, this can be explained by considering distinct simultaneous effects of the ENSO, in both Pallcacocha and Mucubají lakes. Indeed, in the western cordillera of Ecuador, every time an ENSO warm event occurred during the YD and the PB, there was a dominance of more humid climate conditions in this region. That is to say, more frequent and heavy rainfall or snow, a larger input of terrigenous material into the Pallcacocha lake and the consequent lowering of the corresponding *GS* values. Meanwhile, in the Venezuelan Andes, an abnormal increase of the temperature due to an ENSO warm event, taking place during a dry and cool climate period (*Rull et al., 2010*; *Bradbury et al., 1981*; *Curtis et al., 1999*), might have produced an increase of runoff water coming from the glacier mass loss, with a consequent rise of the χ values. Indeed, according to *Francou et al. (2004)*, *Rabatel et*

Table 2. The same as in Table 1, but for Interval 1 (12500 to 10560 cal. yrs BP) and Interval 2 (14770 to 13320 cal. yrs BP).

		χ	S	$SIRM/\chi$
Interval 1				
GS	r	–0.733	–0.544	0.408
	α	**0.000**	**0.000**	**0.000**
Interval 2				
GS	r	0.107	0.014	–0.045
	α	0.185	0.865	0.575

al. (2013) and *Thompson et al. (2011)* the air temperature is the most important factor that influences the retreat of tropical glaciers. Studies of energy balance on the surface of tropical glaciers indicate that higher temperatures favor predominance of rain on snow, which lowers the albedo (*Francou et al., 2004*). Weak winds favor melting over sublimation, and the decrease in cloudiness favors higher incidence of short wavelength radiation (*Francou et al., 2004*; *Rabatel et al., 2013; Thompson et al., 2011*).

On the other hand, the lack of significant correlations between the filtered magnetic parameters and the *GS* observed in Interval 2 could be a sign of the influence of other processes that took place independently in each of these lakes, namely tectonism in Mucubají (*Carrillo et al., 2008*), inner lake dynamics and/or other modes of influence of the climate system.

4.3. Sensitivity of magnetic parameters to variations in *GS*

It is widely accepted, nowadays, that the ENSO events occur when the sea surface temperature anomalies (*SSTA*) shift either above +0.5°C or below –0.5°C, during warm and cold phases, respectively. Assuming that in the past, a similar *SSTA* also led to ENSO occurrences, and that these events were properly recorded in the *GS* from Pallcacocha, we could explore somehow the level of sensitivity of χ, S ratio and $SIRM/\chi$ from Mucubají, to changes of *GS*, and use them as ENSO proxies too. In fact, to determine such sensitivity level, we studied the degree of correlation (Pearson correlation coefficient) between Mucubají magnetic parameters and Pallcacocha *GS* standardized anomalies (*GSSA*), by looking at the latter through windows of different widths that could have mirrored the past record of the *SSTA* (threshold intervals) and the ENSO. We focused our calculations to magnetic data from Interval 1 only.

Figure 6 shows a series of bar charts where the degree of correlation between the *GSSA* and the χ, S ratio and $SIRM/\chi$ magnetic parameters is plotted versus a sequence of threshold intervals. Notice that, in these charts, the Pearson correlation coefficient has been filtered each time through progressively wider threshold intervals or bands of *GSSA*. The minimum interval is (–0.1, 0.1), then their widths are sequentially stretched by discrete increments of (–0.1, 0.1) up to (–1.5, 1.5), covering thus the whole range of *GSSA*.

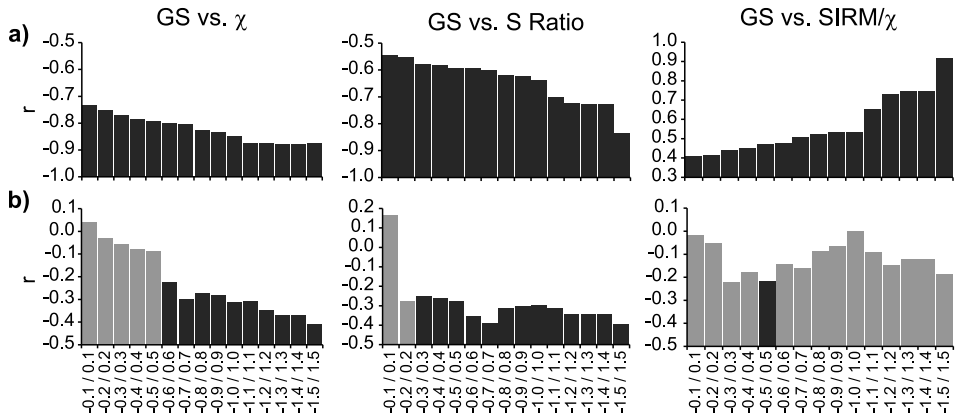

Fig. 6. Bar charts showing the degree of Pearson correlation coefficient *r* obtained for the different magnetic parameters measured in Mucubají, and the gray scale (*GS*) data from Pallcacocha for 12500–10560 cal. yrs BP only. **a)** The correlations are calculated progressively excluding the data within each threshold interval. **b)** The correlations are calculated progressively excluding the data outside each threshold interval. The color of the bars indicates the significance level of these correlations (black: significant in terms of reliability of the estimation procedure; gray: insignificant).

For the first set of bar charts in Fig. 6a, the Pearson coefficients are calculated excluding the data contained within each threshold interval. These charts show that the three magnetic parameters correlate in a significant way, and get progressively better at the tails of the distribution of the *GSSA* values. Indeed, in Fig. 6a it is noticeable that the anti correlations between χ and the *GSSA*, improve up to 14.2% between the minimum Pearson coefficient −0.735, for the more inclusive (−0.1, 0.1) threshold interval, up to −0.877 for the tails outside the *GSSA* distribution, i.e. (−1.3, 1.3) and (−1.4, 1.4). In the same fashion, the correlations with *S* ratio improve to 28.9%, from −0.545 in (−0.1, 0.1), up to −0.834 for the tails of the distribution at (−1.5, 1.5). Finally, there is a positive correspondence with an about 50% of improvement, between $SIRM/\chi$ and the *GSSA*, that goes from 0.407 in (−0.1, 0.1), up to 0.915 in (−1.5, 1.5). These results suggest that the magnetic parameters from Mucubají lake properly respond to changes in the *GSSA* of both signs when they exceed certain thresholds as little as (−0.1, 0.1). This is somehow equivalent to the behavior of the *SSTA* today when it exceeds thresholds of −0.5°C/+0.5°C, triggering changes in the atmospheric tropical circulation.

To better refine our assessment of the sensitivity of these magnetic parameters, to changes of the *GSSA*, we recalculated the correlations of the *GSSA* with the χ, *S* ratio and $SIRM/\chi$, this time excluding the data outside each threshold interval. These results are shown in the bar charts of Fig. 6b. Once more, the correspondence between these values gets better as we progressively include the tails of the distribution. In this case the correlations for χ become significant from the (−0.6, 0.6) interval up to (−1.5, 1.5), with a net improvement of 44.5%. Similarly, for *S*-ratio data, they start to become significant at

(–0.3, 0.3), with a net improvement of 56% at (–1.5, 1.5). In the case of $SIRM/\chi$, our results suggest that this magnetic parameter correlates well, only when the data at the end of the tails, in the *GSSA* distribution, are included, i.e. (–1.5, 1.5). Thus we can argue that the best linear relationship between magnetic parameters measured in Mucubají, and the ENSO proxy from Pallcacocha, occurred when de latter reach the higher values available for the *GSSA*.

In Interval 2, the absence of significant correlations between each of the Mucubají magnetic parameters and their corresponding *GS* values from Pallcacocha, suggests that the paleoclimatic ENSO signal we observed in Interval 1 is not present in Interval 2. Thus, to establish some thresholds for this interval would not provide any relevant information.

4.4. Non linear empirical relationships between the ENSO and magnetic parameters

As a first approach, we used linear correlations to find some empirical connections between the magnetic parameters and the *GS* paleoclimate proxy. Nevertheless, paleoclimate systems usually entail a number of variables that interact to each other in a non-linear and non-random complex way (*Da Silva et al., 2010*; *Peralta et al., 2013*; *Camacho et al., 2013*). Hence, our next step, was to apply an ANFIS to find a family of fuzzy rules (empirical relationships) that could link, for the various subgroups of experimental data points, magnetic data (Mucubají) with the ENSO (Pallcacocha) proxies.

In order to train our fuzzy model, we used the *GS* from Pallcacocha as output and χ, *S* ratio and $SIRM/\chi$ from Mucubají, as input variables. We introduced the training data as sets of one (either χ, *S* ratio or $SIRM/\chi$), two (χ and either *S* ratio or $SIRM/\chi$, or *S* ratio and $SIRM/\chi$) and three (χ, *S* ratio and $SIRM/\chi$) independent input variables and carried out numerous computational trials. Tests were also performed using different combinations and numbers of fuzzy rules. However, to avoid an overtraining of the system, we limited the maximum number of fuzzy rules to 10% of the number of data sets or samples used. The system was trained with 50% of the input data (97 and 78 samples for Interval 1 and 2, respectively) that were chosen randomly and evenly distributed along the Mucubají section. The output (inferred *GS*) was compared with the observed values using scatter plots, and the quality of the inference was quantified using the coefficient of determination r^2 and the root mean-square error (*RMSE*). Table S1 in Electronic Supplement summarizes, for Intervals 1 (Fig. 6a) and 2 (Fig. 6b), the *RMSE* and r^2 obtained after inferring over the whole (100%) data, for all the possible FIS structures, and with a maximum number of 8 fuzzy rules (approximately the 10% of the number of vectors used to train the system). From this table, it is clear that by increasing the number of fuzzy rules we do not necessarily improve the corresponding inferences. In this table we also highlighted, for each interval, the five structures with lower *RMSE*. Table S2 in Electronic Supplement shows the best inferences including their FIS structures and their corresponding fuzzy rules. The best fit for Interval 1 is the structure [3χ 1*S* ratio] with an *RMSE* of 2.556, while for Interval 2 the best fit was obtained with the structure [7χ] with a *RMSE* of 2.025. Figure 7 compares these two best inferences for both intervals. Solid lines stand for the inferred data whereas the circles represent the values corresponding to the actual *GS* from Pallcacocha lake.

In Interval 1 (Fig. 7a), for the age range between approximately 12300 and 12100 cal. yrs BP, the system fails to produce a good inference of the observed data. In a stratigraphic review of some Mucubají logs, *Carrillo et al. (2008)* pointed out that a sequence of silt laminations, interbedded with layers of silty clay rich in organic content, accumulated along this time period. Indeed, according to Fig. 4, the magnetic parameters measured in Mucubají do not seem to show any anomalous behavior within 12300 and 12100 yrs. Thus, any signal related to a climate or to a tectonic event, that could have occurred during this time interval, was only recorded by the *GS* in Pallcacocha lake sediments.

Figure 7b shows, for Interval 2, a rather poor ability of the system to infer *GS* using χ as the sole input variable. We argue that a low quality inference evidences a lack of a consistent physical correlation between magnetic and *GS* proxies, rather than a problem with our non linear approach. Indeed, according to *Rodbell et al. (1999)*, in strata older than 14000 years (more than 50% of Interval 2) the ENSO signals seem to be almost inexistent.

The difference found between the two intervals reinforces once more the idea that the ENSO is a mode of variability of the climate system that can alter local climate changes (i.e. Venezuelan Andes and Ecuador). To better test the quality of these results, as well as to quantify somehow the ability of the magnetic minerals in these sediments to record paleoclimate events such as the ENSO, we also examined the scatter plots of the five best inferences (i.e. lower *RMSE*) obtained for Interval 1 and the three best inferences obtained for Interval 2. These plots (Figs 8 and 9) display the inferred data versus their corresponding observed values.

In Interval 1 (Fig. 8) it is noteworthy that the data tend to cluster over the line of the best theoretical fit. Taking into account the slope of the fitted lines, it is possible to classify these plots into two groups. Group A includes the scatter plots with FIS structures [3χ], [3χ 1*S* ratio] and [3χ 3*S* ratio 1 $SIRM/\chi$] whose best fitted lines have slopes of about 0.5 (Fig. 8a,b,c). On the other hand, group B encompasses the scatter plots of FIS structures [4χ] and [4χ 2*S* ratio], with slopes of about 0.17 for their corresponding best fitted lines (Fig. 8d,e). It is noticeable that the inferences of those *GS* that lie within the 145 and 155 range, are overestimated by the system when the observed values are lower than 150. In the opposite way, the system tends to underestimate the inferred values when the observed ones are higher than 150. This is particularly remarkable in Group B (Fig. 8d,e) where data distribution is more horizontal. The scatter points, corresponding to the structures of Group A, lie closer to the best fitted line. They also seem to better estimate the extreme values (i.e. *GS* observed values higher than 155 and lower than 145).

On the other hand, the scatter plots of Interval 2 (Fig. 9) show that, in the range of observed *GS*, between 115 and 130, the corresponding inferences yield values between 122 and 125. In this case, the system overestimates the *GS* whose observed values are below 123, whereas observed values higher than 123 are underestimated.

Similarly to the case of the linear correlations we argue that, at least for Interval 1, non linear correlations between magnetic parameters and *GS* get better when we use the extreme values (i.e. highest or lowest) in the tails of a hypothetical distribution of *GS*. In the same manner, they worsen when only the central values of the distribution are used. Thus, it seems that the ENSO signal has been better recorded, as a paleoclimate record,

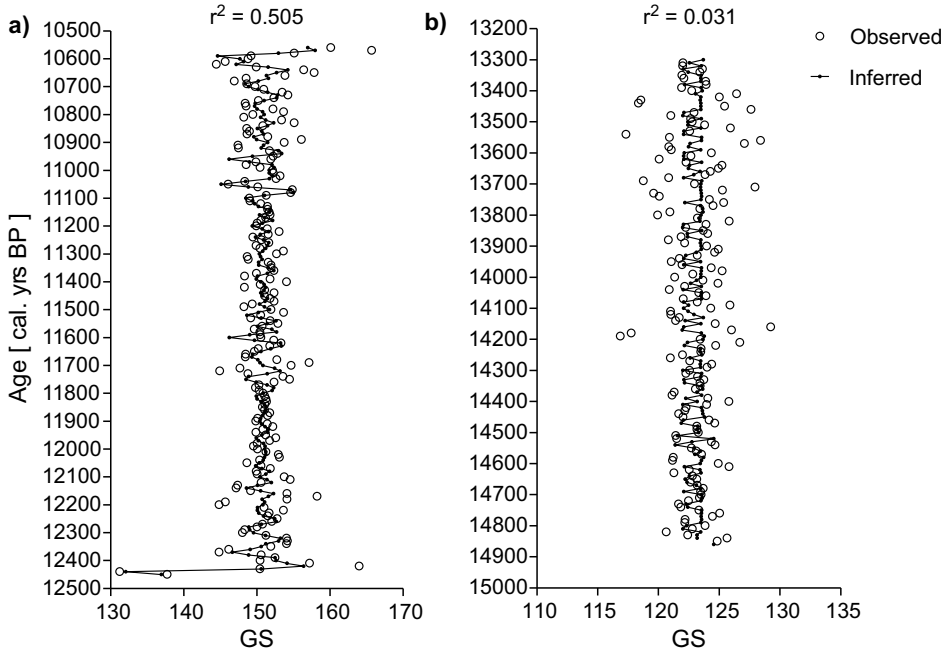

Fig. 7. The best Adaptive Neuro Fuzzy Inference System (ANFIS) inferences for the filtered gray scale (*GS*), after training the system with 50% randomly chosen datasets of filtered magnetic parameters, measured along the combined MUCL 01-02 section. **a)** 3 fuzzy rules were used for the structure [3χ 1*S* ratio] (*RMSE* = 2.556) for 12500–10560 cal. yrs BP, and **b)** 7 fuzzy rules were used for the structure [7χ] (*RMSE* = 2.025) for 14770–13320 cal. yrs BP. Solid curves represent the inferred data whereas the circles represent the observed *GS* mean values from the Pallcacocha record.

when it exceeds certain thresholds of anomalous *GS* values (approximately $-0.4 > GS > +0.4$). From these thresholds upwards, clear cut relationships between the Mucubají lake magnetic records and the *GS* paleoclimate proxies come out.

These relationships also suggest that there was an influence of the ENSO in the Venezuelan Andes during Late Pleistocene times. Such a finding is equivalent to that observed today with the *SSTA*, namely these anomalies should be out of range from their neutral conditions ($-0.5°C > SSTA > +0.5°C$) during certain period of time, so there would be an atmospheric response capable of producing alteration in the pattern of temperature and rain in the Mucubají area. Moreover, regional effects such as tectonism and life-related processes in the lake, may have also obliterated the ENSO paleoclimate record.

In any case, it is noteworthy that the optimal *GS* inference, using a FIS structure [3χ, 1*S* ratio] for Interval 1, with $r^2 = 0.50$ and *RMSE* = 2.55, explains 50.5% of the total variance of the *GS* values, which is equivalent to the total variance of temperature explained by the ENSO nowadays in the Merida Airport Meteorological Station. In fact, previous research, using historic meteorological data for the last 100 years, have explored

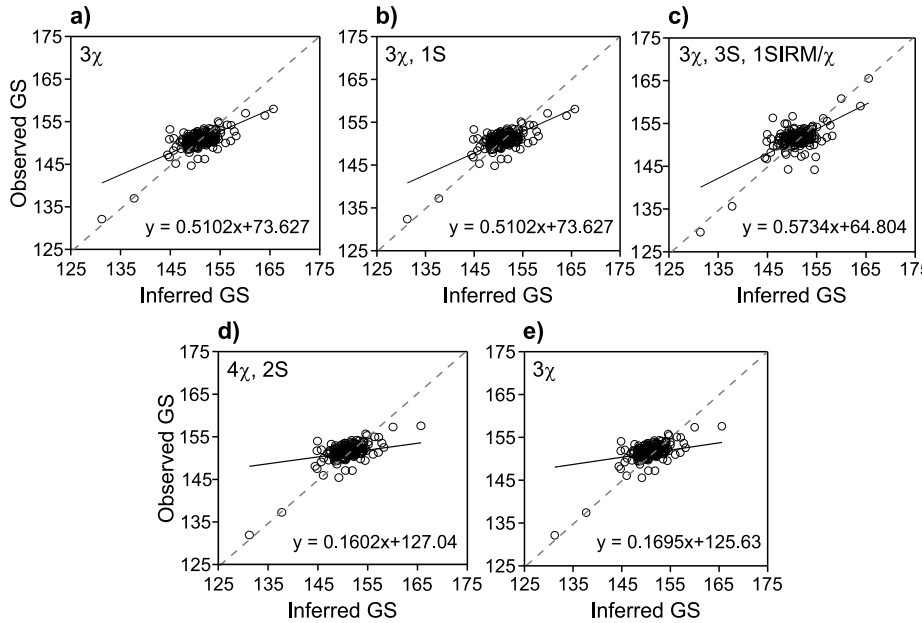

Fig. 8. Scatter plots of observed versus inferred gray scale (*GS*) for 12500–10560 cal. yrs BP with FIS structures **a)** $[3\chi]$, **b)** $[3\chi\ 1S]$ and **c)** $[3\chi\ 3S\ 1SIRM/\chi]$ (Group A), and **d)** $[4\chi]$ and **e)** $[4\chi\ 2S]$ (Group B).

the influence of the ENSO on the variability of rainfall and temperature for different regions in Venezuela (*Cárdenas et al., 2002,2003*; *Arévalo, 2014*). According to these studies, the ENSO explains a 21.2–26.6% of the total variance of the actual precipitation and a 48.2–51.0% of the total variance of temperature. Therefore the impact of the ENSO on the temperature changes of the Venezuelan Andes, could have been about the same as today during the YD and the PB periods (12450 to 10560 cal. yrs BP).

5. CONCLUSIONS

The reconstruction of the Late Pleistocene paleoclimate framework, obtained in this study from the correlations observed between magnetic proxies and *GS*, using linear regression analyses, is consistent with other approaches that apply paleoclimate proxies of the SST. Moreover, it is also consistent with some models that establish relationships between the climate behavior of the eastern equatorial Pacific, and global changes such as the migration of the ITCZ, variations of the SST and the influence of precessional forcings on the dynamics of the oceans.

Magnetic parameters measured in Mucubají, seemed to record an ENSO signal only for the period between 12500 and 10560 cal. yrs BP (Interval 1). Conversely, in Interval 2 (14770–13320 cal. yrs BP) the lack of correlation between magnetic parameters in Mucubají and paleoclimate proxies in Pallcacocha (*GS*), appear to support *Rodbell et al.*

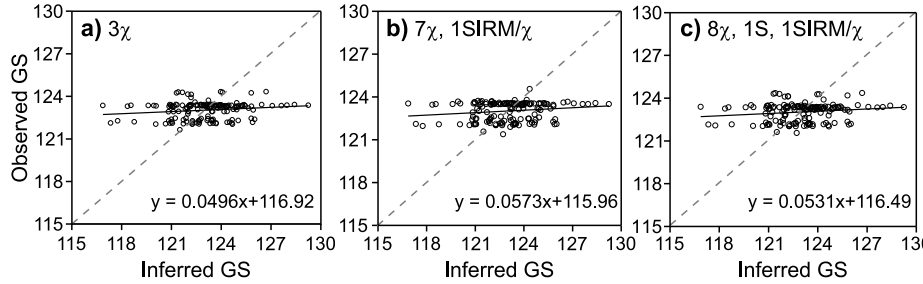

Fig. 9. Scatter plots of observed versus inferred gray scale (*GS*) for 14770–13320 cal. yrs BP with FIS structures **a)** $[3\chi]$, **b)** $[7\chi\ 1SIRM/\chi]$ and **c)** $[8\chi\ 1S\ 1SIRM/\chi]$.

(1999) findings, who argued that during this earlier period the ENSO signal was lost. It is important to point out that, although there are other ENSO proxies such as: corals, ice cores, tree rings, flood deposits and beach ridges (*Rodbell et al., 1999*), high-resolution paleoclimate records for most of them cover the past 2000 years only. In contrast, the *GS* is a high-resolution and tailor-made ENSO proxy, for the tropical Pacific region, that covers a longer time span as the one analyzed here.

We also used a non linear approach (i.e. ANFIS) to look at the possible correlations between magnetic parameters from Mucubají and *GS* paleoclimate proxies from Pallcacocha. The optimal *GS* inference for Interval 1 explains 50.5% of the total variance of the *GS* values (i.e. approximately the actual variance of temperature due to the ENSO in the Venezuelan Andes) indicating that the influence of the ENSO on the temperature changes of this region, between 12500 and 10560 cal. yrs BP, could have been more or less the same as today.

Correlations between magnetic parameters and *GSSA* improve when the extreme values (i.e. highest or lowest) of the *GSSA* are used. Moreover, in order to be recorded by the Mucubají magnetic proxies, the ENSO signal has to exceed certain thresholds of *GSSA* values (approximately $-0.4 > GS > +0.4$). That is consistent with today global climate behavior that requires that the *SSTA* would be out of their neutral temperature conditions ($-0.5°C > SSTA > +0.5°C$), in order to have an atmospheric response capable of producing global climate impacts.

The study of the relationship between these paleoclimate results, and the present behavior of this mode of natural variability in the climate system, is important because its possible implications in the understanding of upcoming global climate changes. That is to say, that the ENSO will continue to influence the natural variability of precipitation and temperature, in the Venezuelan Andes, and in the rest of the country.

Aknowledgments: We would thank the logistic support provided by C. Campos (Universidad Simón Bolívar, Venezuela) and C. Beck (Université de Savoie, France). We also thank the constructive and enriching comments by H. Groening, (Universidad Simón Bolívar). This research was partially funded by LOCTI research grants to V. C.-A. and M. A.

Electronic Supplement - Tables S1 and S2 - can be obtained from
http://www.ig.cas.cz/sites/default/files/u241/costanzo_2016_0024_supplementary_data_pdf_13134.pdf

References

Arévalo J.A., 2014. *Encontrando la señal del ENOS en sedimentos lacustres del Pleistoceno Tardío.* MSc Thesis. Universidad Simón Bolívar, Caracas, Venezuela (in Spanish).

Bradbury P.J., Leyden B., Salgado-Labouriau M., Lewis W.M., Schubert C., Binford M.W., Frey D.G., Whitehead D.R. and Weibezahn F.H., 1981. Late Quaternary environmental history of Lake Valencia, Venezuela. *Science*, **214**, 1299–1305.

Bloemendal J., King J.W., Hall F.R. and Doh S.J., 1992. Rock magnetism of Late Neogene and Pleistocene deep-sea sediments: relationship to sediment source, diagenetic processes and sediment lithology. *J. Geophys. Res.*, **97**, 4361–4375.

Bronk Ramsey C., 2001. Development of the radiocarbon calibration program OxCal. *Radiocarbon*, **43**, 355–363.

Cane M.A., 2005. The evolution of El Niño, past and future. *Earth Planet. Sci. Lett.*, **230**, 227–240.

Caraco N.F., Cole J.J. and Linkens G.E., 1989. Sulfate control of phosphorus availability in lakes. *Hydrobiologia*, **253**, 275–280.

Cárdenas P., García L., Gil A. and Martelo M., 2003. *Impactos de Eventos El Niño-Oscilación del Sur en Venezuela Parte II.* Corporación Andina de Fomento, Caracas, Venezuela (in Spanish).

Cárdenas P., Gil A. and García L., 2002. *Impactos de los eventos El Niño Oscilación del Sur en Venezuela. Parte I.* Corporación Andina de Fomento, Caracas, Venezuela (in Spanish).

Carrillo E., 2006. *L'enregistrement sédimentaire de la sismicité récente le long de la frontière sudoccidentale de la plaque Caraïbe (faille de Boconó): modalités et chronologie. Contribution à l'estimation de l'aléa sismique regional*. PhD Thesis. Université de Savoie, Chambery, France (in French).

Carrillo E, Beck A., Audemard F.A., Moreno E. and Ollarves R., 2008. Disentangling Late Quaternary climatic and seismo-tectonic controls on Lake Mucubají sedimentation (Mérida Andes, Venezuela). *Palaeogeogr. Palaeoclimatol. Palaeoecol.*, **259**, 284–300.

Clement A.C., Cane M.A. and Seager R., 2001. An orbitally driven tropical source for abrupt climate change. *J. Climate*, **14**, 2369–2375.

Clement A.C., Seager R. and Cane M.A., 1999. Orbital controls on the El Niño/Southern Oscillation and the tropical climate. *Paleoceanography*, **14**, 441–456.

Clement A.C., Seager R. and Cane M.A., 2000. Suppression of El Niño during the mid-Holocene by changes in the Earth's orbit. *Paleoceanography*, **15**, 731–737.

Curtis J.H., Brenner M. and Hodell D.A., 1999. Climate change in the Lake Valencia Basin, Venezuela, 12600 yr BP to present. *Holocene*, **9**, 609–619.

Da Silva A., Costanzo-Álvarez V., Hurtado N., Aldana M., Bayona G., Guzmán O. and López-Rodríguez D., 2010. Study of a possible correlation between Miocene global climatic changes and magnetic proxies δ18O, using neuro fuzzy logic analysis: stratigraphic well Saltarín 1A (Llanos foreland basin, Colombia. *Stud. Geophys. Geod.*, **54**, 607–631.

Demicco R.V., 2004. Fuzzy logic and Earth science: an overview. In: Demico R.V. and Klir G.J., (Eds), *Fuzzy Logic in Geology*. Elsevier Science, San Diego, CA, 63–102.

DeWitt D.G. and Schneider E. K., 2000. The tropical ocean response to a change in solar forcing. *J. Climate*, **13**, 1133–1149.

Duchon C.E. and Hale R., 2012. *Time Series Analysis in Meteorology and Climatology: An Introduction.* Wiley-Blackwell, Chichester, West Sussex, UK.

Duan Z., Liu Q., Yang X., Gao X. and Su Y., 2014. Magnetism of the Huguangyan Maar Lake sediments, Southeast China and its paleoenvironmental implications. *Palaeogeogr. Palaeoclimatol. Palaeoecol.*, **395**, 158–167.

Finol J. and Jing X.D., 2002. Predicting petrophysical parameters in a fuzzy environment in soft computing for reservoir characterisation and modeling. In: Wong P., Aminzadeh F. and Nikravesh M. (Eds), *Soft Computing for Reservoir Characterization and Modeling*. Studies in Fuzziness and Soft Computing, **80**, Physica-Verlag, Heidelberg, Germany, 183–217.

Francou B., Vuille M., Favier V. and Cáceres B., 2004. New evidence for an ENSO impact on low-latitude glaciers: Antizana 15, Andes of Ecuador, 0°28′S. *J. Geophys. Res.*, **109**, D18106, DOI: 10.1029/2003JD004484.

Frank U. and Nowaczyk N.R., 2008. Mineral magnetic properties of artificial samples systematically mixed from haematite and magnetite. *Geophys. J. Int.*, **175**, 449–461.

Haug G.H., Hughen K.A., Sigman D.M., Peterson L.C., and Röhl, U., 2001. Southward migration of the Intertropical Convergence Zone through the Holocene. *Science*, **293**, 1305–1308.

Hayashida A., Nakano R., Nagashima A., Seto K., Yamada K. and Yonenobu H., 2015. Magnetic properties of surficial sediments in Lake Ogawara on the Pacific coast of northeastern Japan: spatial variability and correlation with brackish water stratification. *Earth Planets Space*, **67**, 171, DOI: 10.1186/s40623-015-0343-7.

Hu S.Y., Wang S.M. and Appel E., 2000. The environmental mechanism of fluctuations of magnetic susceptibility recorded in lacustrine sediments from Jalai Nur, Inner Mongolia. *Sci. China Ser. D - Earth Sci*., **43**, 534–540.

Hurtado N., Aldana M. and Torres J., 2009. Comparison between neuro-fuzzy and fractal models for permeability prediction. *Comput. Geosci.*, **13**, 181–186.

Kent D.V., 1982. Apparent correlation of palaeomagnetic intensity and climatic records in deep-sea sediments. *Nature*, **299**, 538–539.

Kienast M., Kienast S.S., Calvert S.E., Eglinton T.I., Mollenhauer G., Francois R. and Mix A.C., 2006. Eastern Pacific cooling and Atlantic overturning circulation during the last deglaciation. *Nature*, **443**, 846–849.

Koutavas A., Lynch-Stieglitz J., Marchitto T.M. and Sachs J.P., 2002. El Niño-like pattern in ice age tropical Pacific sea surface temperature. *Science*, **297**, 226–230.

Li Y.X., Yu Z., Kodama K.P. and Moeller R.E., 2006. A 14,000-year environmental change history revealed by mineral magnetic data from White Lake, New Jersey, USA. *Earth Planet Sci. Lett*., **246**, 27–40.

Liu Q., Roberts A.P., Torrent J., Horng C.-S. and Larrasoaña J.C., 2007. What do the HIRM and S-ratio really measure in environmental magnetism? *Geochem. Geophys. Geosyst.*, **8**, Q09011, DOI: 10.1029/2007GC001717.

Moy M., Seltzer G., Seltzer D. and Anderson D., 2002. Variability of El Nino/Southern Oscillation activity at millennial time scales during the Holocene epoch. *Nature*, **420**, 162–165.

Nriagu J.O., 1972. Stability of vivianite and ion-pair formation in the system $Fe_3(PO_4)_2$-H_3PO_4-H_2O. *Geochim. Cosmochim. Acta*, **36**, 459–470.

Nriagu J.O. and Dell C.I., 1974. Diagenetic formation of iron phosphates in recent lake sediments. *Am. Mineral.*, **59**, 934–946.

Otto-Bliesner B.L., Brady E.C., Clauzet G., Tomas R., Levis S. and Kothavala Z., 2006. Last glacial maximum and Holocene climate in CCSM3. *J. Climate*, **19**, 2526–2544.

Peralta A., Costanzo-Álvarez V., Carrillo E., Durán L.E., Aldana M. and Rey D., 2013. Numerical relationships between magnetic parameters measured in Quaternary sediments and global paleoclimatic proxies. *Stud. Geophys.Geod.*, **57**, 647–668.

Peters C. and Dekkers M.J. 2003. Selected room temperature magnetic parameters as a function of mineralogy, concentration and grain-size. *Phys. Chem. Earth*, **28**, 659–667.

Polissar P.J., Abbott M.B., Wolfe A.P., Bezada M., Rull V. and Bradley R.S. 2006. Solar modulation of Little Ice Age climate in the tropical Andes. *Proc. Natl. Acad. Sci. U. S. A.*, **103**, 8937–8942.

Quinn W.H. and Neal V.T., 1992. The historical record of El Nino events. In: Bradley R.S. and Jones P.D. (Eds), *Climate since A.D. 1500*. Routledge, London, U.K., 623–648.

Rabatel A., Francou B., Soruco A., Gomez J., Cáceres B., Ceballos J. L., Basantes R., Vuille M., Sicart J.-E., Huggel C., Scheel M., Lejeune Y., Arnaud Y., Collet M., Condom T., Consoli G., Favier V., Jomelli V., Galarraga R., Ginot P., Maisincho L., Mendoza J., Ménégoz M., Ramirez E., Ribstein P., Suarez W., Villacis M. and Wagnon P., 2013. Review article of the current state of glaciers in the tropical Andes: a multi-century perspective on glacier evolution and climate change. *Cryosphere Discussions*, **6**, 2477–2536.

Rajaee T., Mirbagheri S.A., Nourani V. and Alikhani A., 2010. Prediction of daily suspended sediment load using wavelet and neuro fuzzy combined model. *Int. J. Environ. Sci. Technol.*, 7, 93–110.

Rodbell D., Seltzer G., Anderson D., Abbott M., Enfield D. and Newman J.H., 1999. An ~15,000-year record of El Niño-driven alluviation in Southwestern Ecuador. *Science*, **283**, 516–520.

Ropelewski C.F. and Halpert M.S., 1987. Global and regional scale precipitation patterns associated with the El Niño-Southern Oscillation. *Mon. Weather Rev.*, **115**, 1606–1626.

Rull V., Stansell N., Montoya E., Bezada M. and Abbott M., 2010. Palynological signal of the Younger Dryas in the tropical Venezuelan Andes. *Quat. Sci. Rev.*, **29**, 3045–3056.

Sagnotti L., 2007. Iron sulfides. In: Gubbins D. and Herrera-Bervera E. (Eds), *Encyclopedia of Geomagnetism and Paleomagnetism*. Springer-Verlag, Heidelberg, Germany, 454–459.

Shackleton N.J. and Opdyke N.D., 1973. Oxygen isotope and paleomagnetic stratigraphy of equatorial Pacific core V28-238: Oxygen isotope temperatures and ice volumes on a 105-year and 106-year scale. *Quat. Res*, **3**, 39–55.

Singh U.K., Singh D.K. and Singh H., 2010. Application of neuro fuzzy pattern recognition method in borehole geophysics. *Acta Geod. Geophys. Hung.*, **45**, 417–425.

Stansell N.D., Abbott M.B., Polissar P.J., Wolfe A.P., Bezada M. and Rull V., 2005. Late Quaternary deglacial history of the Mérida Andes, Venezuela. *J. Quat. Sci.*, **20** ,801–812.

Stansell N.D., Abbott M.B., Rull V., Rodbell D., Bezada M and Montoya E., 2010. Abrupt Younger Dryas cooling in the northern tropics recorded in lake sediments from the Venezuelan Andes. *Earth Planet. Sci. Lett.*, **293**, 154–163.

Stuiver M., Reimer P.J., Bard E., Beck J.W., Burr G. S., Hughen K.A., Kromer B., McCormac K.A., Van Der Plicht J. and Spurk M., 1998. INTCAL 98 radiocarbon age calibration, 24,000-0 cal BP. *Radiocarbon*, **40**, 1041–1083.

Stott L., Poulsen C., Lund S. and Thunell R., 2002. Super ENSO and global climate oscillations at millennial time scales. *Science*, **297**, 222–226.

Su Y.L., Gao X., Liu Q.S., Hu P.X., Duan Z.Q., Jiang Z.X.,Wang J.B., Zhu L.P., Doberschütz S., Mäusbacher R., Daut G. and Haberzettl T., 2013. Mechanism of variations in environmental magnetic proxies of lake sediments from Nam Co, Tibet during the Holocene. *Chinese Sci. Bull.*, **58**, 1568–1578, DOI: 10.1007/s11434-012-5324-7.

Tahmasebi P. and Hezarkhani A., 2010. Application of Adaptive Neuro-Fuzzy Inference System for grade estimation; case study, Sarcheshmeh porphyry copper deposit, Kerman, Iran. *Aust. J. Basic Appl. Sci.*, **4**, 408–420.

Tamuntuan G., Bijaksana S., Gaffar E., Russell J., Safiuddin L.O. and Huliselan E., 2010. The magnetic properties of Indonesian lake sediment: A case study of a tectonic lake in South Sulawesi and Maar Lakes in East Java. *ITB J. Sci*., **42A**, 31–48.

Thompson L.G., Mosley-Thompson E., Davis M.E. and Brecher H.H., 2011. Tropical glaciers, recorders and indicators of climate change, are disappearing globally. *Ann. Glaciol*., **52**, 23–34.

Timmermann A., Lorenz S.J., An S.-I., Clement A. and Xie S.-P., 2007. The effect of orbital forcing on the mean climate and variability of the tropical Pacific. *J. Climate*, **20**, 4147–4159.

Wang H., Liu H., Liu Y., Cui H. and Abrahamsen N., 2010. Mineral magnetism and other characteristics of sediments from an alpine lake (3,410 m a.s.l.) in central China and implications for late Holocene climate and environment. *J. Paleolimnol.*, **43**, 345–367, DOI: 10.1007/s10933-009-9335-6.

Zhang R. and Delworth T.L., 2005. Simulated tropical response to a substantial weakening of the Atlantic thermohaline circulation. *J. Climate*, **18**, 1853–1860.

Zhang W., Appel E., Fang X., Yan M., Song Ch. and Cao L., 2012. Paleoclimatic implications of magnetic susceptibility in Late Pliocene–Quaternary sediments from deep drilling core SG-1 in the western Qaidam Basin (NE Tibetan Plateau). *J. Geophys. Res.*, **117**, B06101, DOI: 10.1029/2011JB008949.

Ziaii M., Pouyan A.A. and Ziaei M., 2009. Neuro-fuzzy modelling in mining geochemistry: Identification of geochemical anomalies. *J. Geochem. Explor.*, **100**, 25–36.

Zoveidavianpoor M., Samsuri A. and Shadizadeh S.R., 2013. Adaptive neuro fuzzy inference system for compressional wave velocity prediction in a carbonate reservoir. *J. Appl. Geophys.*, **89**, 96–107.